www.advmatinterfaces.de

# Regio-Selective Functionalisation of Electrospun Materials at the Microscale

Marius Schmidt, Carina Riecken, Eyal Zussman, Seema Agarwal, Holger Schmalz, and Andreas Greiner\*

Electrospun nonwovens are highly versatile materials. Significant progress is achieved in terms of materials, methods, and setups, enabling a wide range of applications. However, regio-selective surface modification of electrospun fibers along their longitudinal axes remains an open challenge. This paper addresses this challenge and presents side-by-side electrospinning as a straightforward method for producing functional bead-on-string (BOS) fibers. The functional beads carry tertiary amino groups as a platform for further modifications. The beads are arranged in recurring distances along the fiber, allowing a precise fiber modification on the micron scale. This arrangement has been used for modifications with a fluorescent dye and gold nanoparticles (AuNP) in a highly precise and regio-selective manner. AuNP decorated BOS fiber nonwovens show excellent performance as heterogenous catalysts under flow conditions demonstrating low pressure drop, high turnover frequency, and recyclability.

1. Introduction

Electrospun nonwovens offer high surface area-to-volume ratios, adjustable porosity, and mechanical flexibility.<sup>[1]</sup> They are particularly appealing for applications in fields like biomedical engineering,<sup>[2]</sup> filtration,<sup>[3]</sup> energy storage,<sup>[4]</sup> and as support material for heterogeneous catalysis.<sup>[5]</sup> Despite their intrinsic advantages, the potential of electrospun fibers could be further increased through regio-selective surface modification to obtain

M. Schmidt, C. Riecken, S. Agarwal, H. Schmalz, A. Greiner Macromolecular Chemistry
University of Bayreuth
Universitätsstrasse 30, 95447 Bayreuth, Germany
E-mail: andreas.greiner@uni-bayreuth.de
E. Zussman
Faculty of Mechanical Engineering
Technion—Israel Institute of Technology
Haifa 3200003, Israel
S. Agarwal, H. Schmalz, A. Greiner
Bayarian Polymer Institute

Universitätsstrasse 30, 95447 Bayreuth, Germany

The ORCID identification number(s) for the author(s) of this article can be found under https://doi.org/10.1002/admi.202400666

© 2024 The Author(s). Advanced Materials Interfaces published by Wiley-VCH GmbH. This is an open access article under the terms of the Creative Commons Attribution License, which permits use, distribution and reproduction in any medium, provided the original work is properly cited.

DOI: 10.1002/admi.202400666

fibers with spatially distinct surfaces having different chemical functionalities. One efficient method to produce these fibers is side-by-side electrospinning, which combines two materials with distinct properties in one fiber.[6] This method is commonly used to produce Janus (or side-by-side) fibers that feature a phase-separated structure with two sides (faces) made of different materials running parallel to the fiber's long axis.[7] This unique structure can be harnessed to introduce anchor groups in one side of the Janus fibers for the regio-selective incorporation of gold nanoparticles (AuNP),[8] to construct iniectable extracellular matrices.[9] or as water harvesting systems.[10] Combining hydrophobic and hydrophilic polymers with a high boiling solvent for

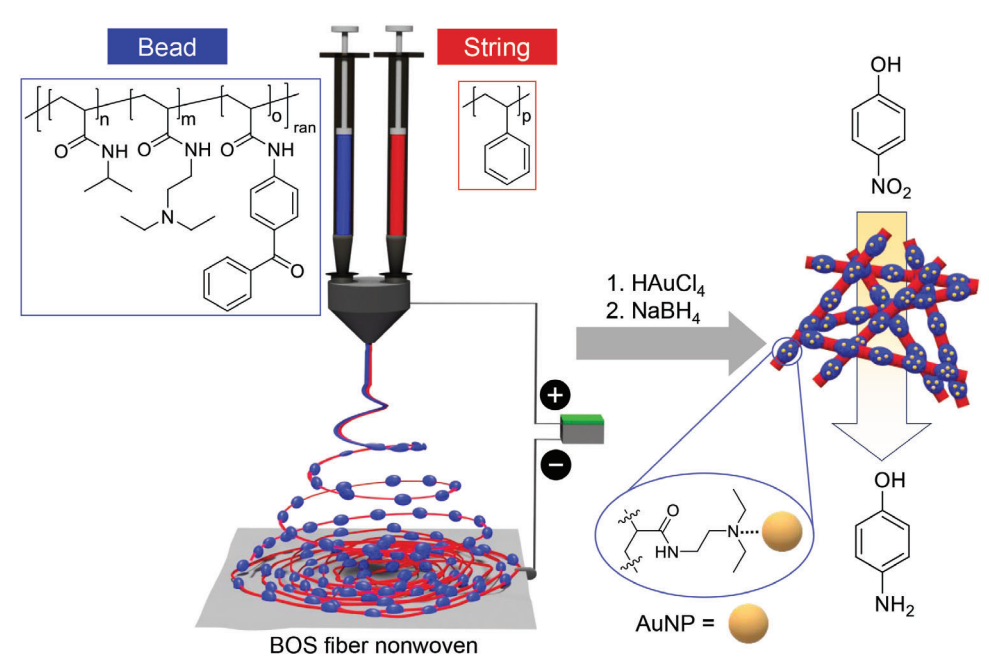
side-by-side electrospinning opens access to bead-on-string (BOS) fibers with a highly recurring arrangement of hydrophilic beads on a hydrophobic core fiber. BOS fibers have been fabricated by Gernhardt et al. using dimethylformamide (DMF) solutions of poly(methyl methacrylate-co-butyl methacrylate) as core and poly(N-isopropyl acrylamide) (PNIPAM) as bead material. <sup>[11]</sup> The formation of beads is driven by the Plateau-Rayleigh instability, which leads to the break-up of the jet containing the polar, hydrophilic polymer. <sup>[12]</sup> An important prerequisite is a sufficiently high incompatibility (difference in Hildebrand solubility parameter) to the nonpolar polymer forming the fiber core. Additionally, solvents with high boiling points are essential to allow sufficient time for bead formation before solidification as otherwise Janus fibers will be preferentially formed. <sup>[11]</sup>

BOS fiber nonwovens with hydrophobic and hydrophilic, swellable parts could be interesting as a support material in heterogeneous catalysis, particularly when operating under flow conditions. A support material for a heterogeneous catalyst should ensure high accessibility of the reactants to the catalyst surface in the reaction medium, which can be achieved by swelling the support material. Furthermore, when operating under flow conditions, it is essential that the pressure drop across the membrane remains low during the reaction; otherwise, a significant amount of energy is required. However, swelling increases the fiber diameter resulting in shrinkage of the pore size which results in high pressure drops across the membrane.<sup>[13]</sup> We expect lower pressure drop in BOS fibers with hydrophobic and hydrophilic, swellable parts compared to pure

www.advancedsciencenews.com



www.advmatinterfaces.de



**Scheme 1.** Preparation of functional BOS fibers via side-by-side electrospinning, their regio-selective decoration with AuNP, and application as heterogenous catalyst under flow conditions for the reduction of 4-nitrophenol. The pendant tertiary amino groups in the PIDB beads of the BOS fibers allow their regio-selective decoration with AuNP.

hydrophilic, swellable fibers. The gap between the beads could reduce the shrinkage of the pores. Furthermore, for air filtration, it was demonstrated that BOS nanofibrous membranes exhibit enhanced permeability and reduced pressure drop.<sup>[14]</sup>

In this study, we have prepared BOS fibers with hydrophilic, functional beads arranged in recurring distances on a hydrophobic polystyrene (PS) core. This design enabled regio-selective modification with AuNPs with high precision on the micron scale, making them suitable for use as heterogeneous catalysts under flow conditions (Scheme 1).

Due to the combination of hydrophilic, swellable beads with a hydrophobic core, BOS fiber nonwovens decorated with AuNP exhibited exceptional performance as heterogeneous catalysts under flow conditions. These nonwovens achieved low-pressure drop and turnover frequencies (TOF) up to  $\approx 90~h^{-1}$ .

## 2. Results and Discussion

### 2.1. Polymer Synthesis and Fiber Preparation

For the bead material a random copolymer of N-isopropylacrylamide (NIPAM) with N,N-(2-(diethylamino)ethyl)acrylamide (DEAAm) and N-(4-benzovlphenyl)acrylamide (BPAA), denoted as PIDB in the following, was used. PNIPAM as the main component of the bead material has a high Hildebrand solubility parameter ( $\delta = 22.1 \text{ MPa}^{1/2}$ ),[15] which ensures sufficient incompatibility with the PS core fiber ( $\delta = 18.4 \text{ MPa}^{1/2}$ )[16] to facilitate bead formation upon side-by-side electrospinning. The DEAAm units provide functional tertiary amino groups for selective surface modification with AuNP. BPAA was introduced to enable UV-crosslinking to make the fiber stable in an aqueous solution. PIDB was prepared through free radical copolymerization of NIPAM, N-acryloxysuccinimide (NASI), and BPAA, followed by post-modification of the NASI active ester units with N,N-diethylenediamine (DEA; Scheme \$1, Supporting Information). Kinetic studies revealed an almost constant copolymer composition over time proving the random nature of the copolymerization (Figure S5, Supporting Information). The composition of the obtained P(NIPAM-co-NASI-co-BPAA) was NIPAM:NASI:BPAA = 62:30:8 mol% as revealed by proton nuclear magnetic resonance (1H-NMR) spectroscopy (Figure S6, Supporting Information). To introduce pendant tertiary amino groups, DEA was reacted with the precursor copolymer. In the Fourier-transform infrared (FT-IR) spectrum, the esterand imide-vibrations of NASI completely disappeared, demonstrating a full conversion (Figure S7, Supporting Information). This is also confirmed by <sup>1</sup>H-NMR by the disappearance of NASI-specific peaks and the appearance of new peaks that can be assigned to the introduced pendant N,N-diethylamino groups (Figure S6, Supporting Information). Size-exclusion chromatography (SEC) reveals a molecular weight of PIDB of  $M_{\rm n} = 113000$  and a dispersity of D = 2.6 (Figures S8 and S9, Supporting Information).

To identify the optimal electrospinning parameters for producing BOS fibers we conducted a series of experiments varying the concentration and feed rate of the PIDB solution in DMF (**Figure 1** and Table S2, Supporting Information) while the concentration of the PS solution ( $c_{PS} = 27.5$  wt%) and feed rate (0.6 mL h<sup>-1</sup>) remained constant. The PIDB feed rate ranged from 0.3 to 1.2 mL h<sup>-1</sup>, and the concentration was set between  $c_{PIDB} = 15$  and 35 wt%. No BOS fibers were formed for a PIDB concentration of  $c_{PIDB} = 35$  wt%, regardless of the employed feed rate (Figure 1A–D). This is probably caused by the comparably high zero shear viscosity of the solution ( $\eta_0 = 1550$  mPa s) as

www.advancedsciencenews.com



www.advmatinterfaces.de

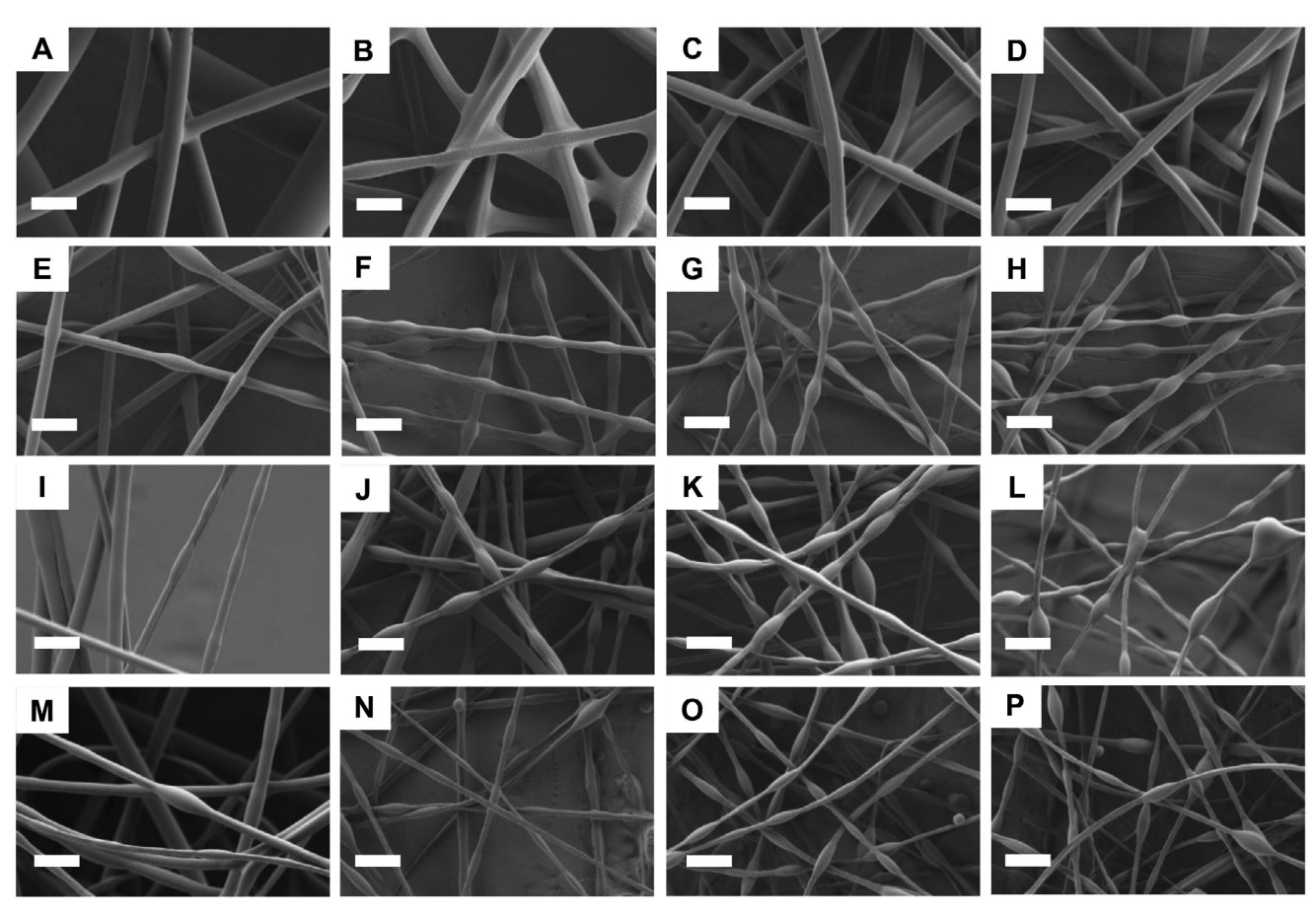


Figure 1. SEM images of fibers prepared by side-by-side electrospinning with varying concentrations and feed rates of the PIDB solution in DMF, while keeping the PS concentration (27.5 wt% in DMF) and feed rate (0.6 mL  $h^{-1}$ ) constant. The scale bar in all images is 5  $\mu$ m. Vertical: Variation of the PIDB concentration. Horizontal: Variation of the PIDB feed rate. A) 35 wt%/0.3 mL  $h^{-1}$ , B) 35 wt%/0.6 mL  $h^{-1}$ , C) 35 wt%/0.9 mL  $h^{-1}$ , D) 35 wt%/1.2 mL  $h^{-1}$ , E) 25 wt%/0.3 mL  $h^{-1}$ , F) 25 wt%/0.6 mL  $h^{-1}$ , G) 25 wt%/0.9 mL  $h^{-1}$ , H) 25 wt%/1.2 mL  $h^{-1}$ , I) 20 wt%/0.3 mL  $h^{-1}$ , J) 20 wt%/0.6 mL  $h^{-1}$ , K) 20 wt%/0.9 mL  $h^{-1}$ , D) 15 wt%/0.9 mL  $h^{-1}$ , N) 15 wt%/0.6 mL  $h^{-1}$ , O) 15 wt%/0.9 mL  $h^{-1}$ , and P) 15 wt%/1.2 mL  $h^{-1}$ .

determined by rheology (Figure S10, Supporting Information). This leads to rapid PIDB solidification and prevents the splitting of the jet into beads during fiber formation.

Consequently, we reduced the PIDB concentration to  $c_{\rm PIDB}=25$ , 20, and 15 wt%, resulting in decreased viscosities reaching 49 mPa s for the 15 wt% solution. Scanning electron microscopy (SEM) images revealed bead formation for all PIDB solution concentrations with  $c_{\rm PIDB}=25$ , 20, and 15 wt% with a feed rate of at least 0.6 mL h<sup>-1</sup> (Figure 1E–P). However, droplet formation occurred with the electrospinning solution containing 15 wt% PIDB, along with the formation of very thin fibers. Furthermore, at 20 wt% polymer concentration and 1.2 mL h<sup>-1</sup>, beads appeared partly deformed and merged. To maintain a distinct two-phase system, we chose to proceed with a 20 wt% PIDB concentration. In principle, the feed rate can be adjusted between 0.6 and 0.9 mL h<sup>-1</sup> without compromising fiber morphology quality. We decided to conduct the subsequent experiments with a feed rate of 0.9 mL h<sup>-1</sup>.

The spatial distribution of PS and PIDB in the BOS fibers was analyzed by Raman imaging. From the extracted component distributions shown in **Figure 2A** (x,y scan) and Figure **2B** (bead cross-section), it becomes evident that the core fiber is solely

formed by PS (shown in red). The beads exhibit a core-shell structure with a PS core and PIDB shell (shown in blue). Hence, SEM and Raman imaging confirm the desired BOS structure of the fibers with functional PIDB beads being arranged in recurring distances on the supporting PS core fiber.

As a proof of concept, we investigated the regio-selective binding of a fluorescence dye to the beads. BOS fibers, electrospun onto a glass slide, were immersed in a fluorescein disodium salt solution ( $c=1\,$  mM, pH = 7.2). We assumed that the negative charge at the phenolate and carboxylate groups could promote electrostatic interactions with the tertiary amino groups in the PIDB beads (pKa  $\approx 10$ ), which are partially protonated under the employed conditions (Scheme S2, Supporting Information). The fluorescence microscopy image shown in Figure 2C demonstrates the successful regio-selective modification with fluorescein disodium salt.

## 2.2. Pressure Drop and Catalysis

For the application of the BOS fiber nonwovens in flow catalysis the pressure drop across the nonwoven is a crucial

conditions) on Wiley Online Library for rules of use; OA articles are governed by the applicable Creative Commons

www.advmatinterfaces.de

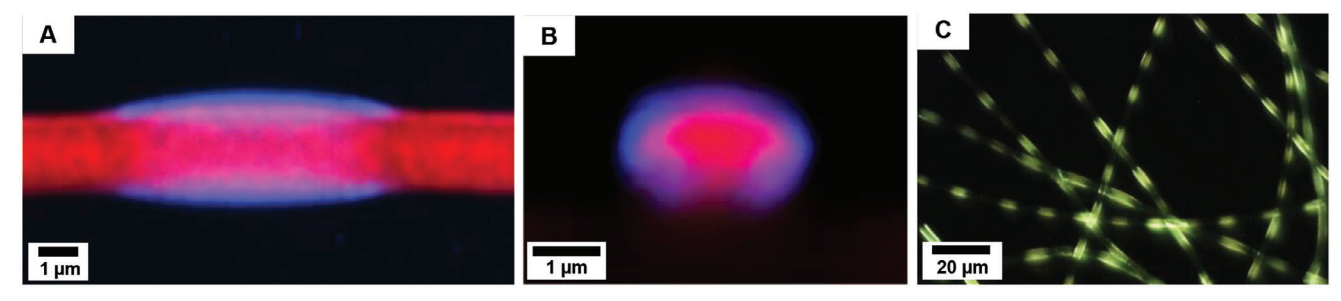


Figure 2. A,B) show the spatial distribution of PS (red) and PIDB (blue) extracted from Raman imaging; the corresponding Raman spectra of the neat components are given in Figure S11 (Supporting Information). C) Fluorescence microscopy image of BOS fibers after immersion in fluorescein disodium salt solution. The PIDB beads show bright fluorescence due to selective interaction with fluorescein disodium salt.

characteristic. Low-pressure drops are preferred because less energy is required to pass the reactants through the mesh. Pressure drop measurements of the BOS fiber nonwovens were conducted and compared to neat PS and PIDB nonwovens that had comparable fiber diameters. The PS and PIDB nonwovens were fabricated with a fiber diameter of  $D_{\rm fiber}=1.08\pm0.15~\mu{\rm m}$  and  $D_{\rm fiber}=1.02\pm0.18~\mu{\rm m}$ , respectively. The diameter of the PS core of the BOS fiber nonwoven was  $D_{\rm core}=1.11\pm0.14~\mu{\rm m}$  and the average bead diameter  $D_{\rm bead}=1.98\pm0.40~\mu{\rm m}$ . The BOS fiber nonwoven shows a very low-pressure drop comparable to that of

the neat PS nonwoven, whereas for the neat hydrophilic PIDB nonwoven the pressure drop is significantly higher (Figure 3A). In general, the pressure drop over a fibrous mesh is strongly affected by its pore size, with decreasing pore sizes resulting in increasing pressure drops.<sup>[16]</sup> Swelling of fibers leads to shrinkage of pores and consequently reduces the flux across the membrane. The pure PIDB nonwoven shows the highest swelling degree, explaining its high-pressure drop (Figure 3B). It appears that the BOS structure almost completely compensates for this effect. We assume the relatively stiff PS segments kept

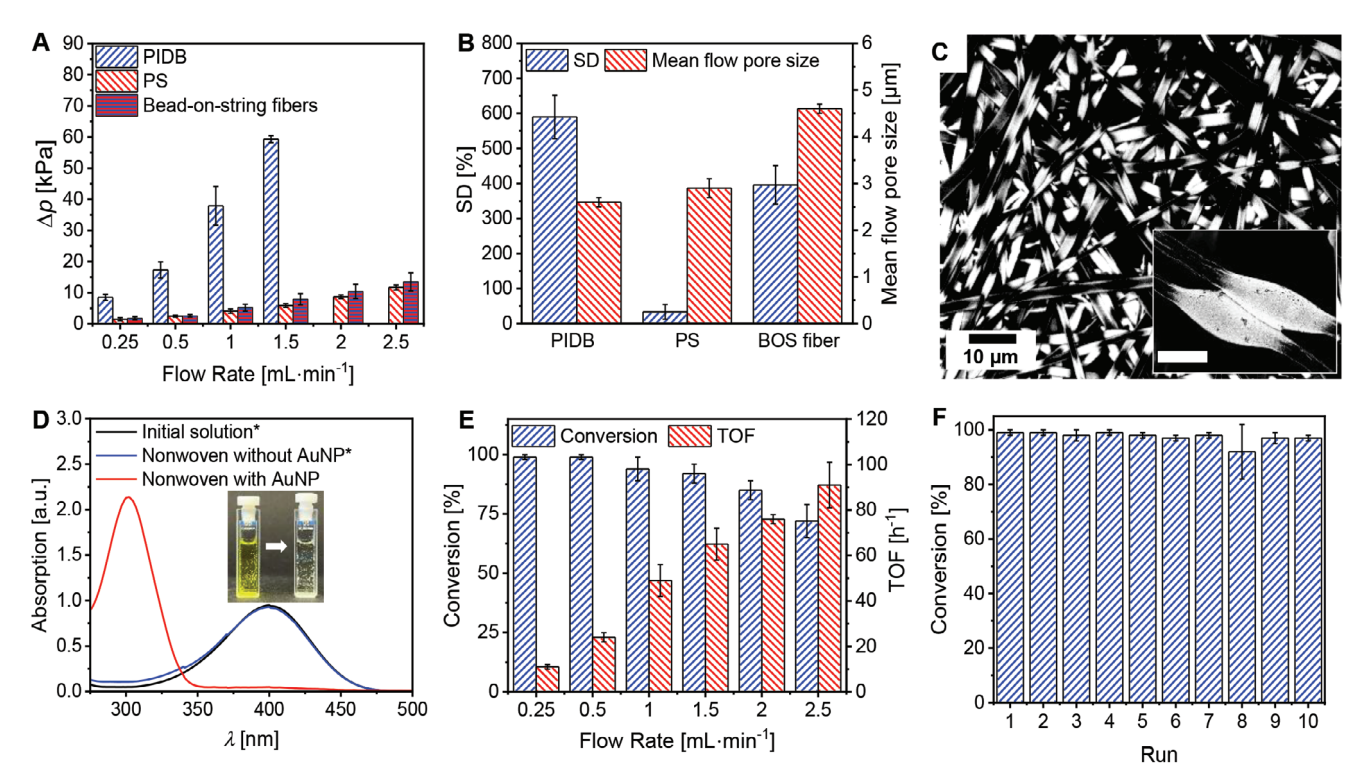


Figure 3. A,B) Comparison of the pressure drop at different flow rates, swelling degree (SD) and mean flow pore size of a PIDB nonwoven, PS nonwoven, and BOS nonwoven. Note: When the pressure drop exceeded 60 kPa, the measurements were stopped because the syringe pump was no longer able to maintain a constant flow rate. C) SEM image of BOS fibers after decoration with AuNP analyzed with a BSE detector. The inset shows two beads in high magnification (15,000x, scale bar =  $2 \mu m$ ). D) UV-vis spectra of the initial 4-nitrophenol solution (c = 1 mM, black), the solution after passing through a BOS nonwoven without (blue) and with AuNP (red). For the UV-vis measurements, the initial solution and the solution after passing through the BOS nonwoven without AuNP were diluted at a ratio of 1:20. The photograph in the inset shows the solution before and after passing the BOS nonwoven with AuNP. The flow rate was 0.25 mL min<sup>-1</sup>. E) Conversion and TOF at different flow rates. F) Recyclability of the BOS nonwovens. Each cycle was conducted at a flow rate of 0.25 mL min<sup>-1</sup>.

**ADVANCED** SCIENCE NEWS

www.advancedsciencenews.com



www.advmatinterfaces.de

the stability of the membrane skeleton and thus preserved the pores' volume/area. Moreover, pore size measurements revealed that the BOS fiber nonwoven has the largest pores (Figure 3B), which agrees well with the observed low-pressure drop. The low pressure drop combined with the large swelling, makes the BOS fiber nonwoven highly suitable for applications in flow catalysis.

To apply the BOS fiber nonwoven in flow catalysis, the beads were selectively decorated with AuNP. To this end, the fibers were immersed in an aqueous tetrachloroauric acid (HAuCl<sub>4</sub>) solution to selectively load the beads with HAuCl<sub>4</sub> via acidbase reaction with the pendant tertiary amino groups. Subsequently, the nonwovens were immersed in an aqueous sodium borohydride (NaBH<sub>4</sub>) solution to induce reduction and formation of AuNP. The successful formation of AuNP on the BOS fiber nonwoven could be directly observed through a color change from slightly yellow to deep red after immersion in the NaBH<sub>4</sub> solution (Figure S12, Supporting Information). According to ICP-OES (inductively coupled plasma-optical emission spectrometry) the adsorption capacity is 77 µg Au per mg of BOS fiber nonwoven (Figure \$13, Supporting Information). The regio-selective decoration of the beads with AuNP was confirmed by SEM using a backscattered electron (BSE) detector (Figure 3C). In the BSE detector images, only the selectively decorated beads appear bright due to the higher contrast of the AuNP (higher atomic number) with respect to the underlying PS core fiber.

The catalytic performance of the AuNP decorated BOS fiber nonwovens was tested employing the reduction of 4nitrophenolate to 4-aminophenolate with NaBH4 as a wellestablished model reaction.<sup>[17]</sup> Monitoring of the conversion is possible via the decrease of the 4-nitrophenolate peak  $(\lambda_{max} = 400 \text{ nm})$  and the increase of the 4-aminophenolate peak  $(\lambda_{\text{max}} = 300 \text{ nm})$ . Figure 3D displays the UV-vis spectra and a photograph of the solutions before (initial 4-nitrophenolate concentration c = 1 mM) and after passing an AuNP-decorated BOS fiber nonwoven at a flow rate of 0.25 mL min<sup>-1</sup>. Full conversion was achieved, as proven by the absence of a peak at  $\lambda = 400$  nm. The conversion remains above 90% at flow rates up to 1.5 mL min<sup>-1</sup> but then declines to 72% at a flow rate of 2.5 mL min<sup>-1</sup> (Figure 3E; Figure S14, Supporting Information). The decrease in conversion with increasing flow rates is due to the short residence time of the reactants in the membrane. [18] TOF values up to 91  $\pm$  11 h<sup>-1</sup> are attained (Figure 3E). The TOF values are notably high compared to those documented in the literature, despite the relatively low flow rate of 2.5 mL min<sup>-1</sup> (Table S3, Supporting Information). The recyclability was investigated by performing ten runs with a flow rate of 0.25 mL min<sup>-1</sup>. Even after ten cycles, the catalytic activity is maintained (Figure 3F). The UV-vis reflectance spectra of the AuNP-decorated BOS fiber nonwoven before and after ten cycles reveal no discernible changes, indicating no agglomeration of AuNP (Figure \$15, Supporting Information). ICP-OES measurements show only minor leaching. The Au-content before flow catalysis decreases from 8.7 to 8.0 wt% after catalysis. These results underscore the effective stabilization of AuNP by PIDB. Furthermore, SEM images taken after ten cycles confirm the morphological stability of the BOS fibers (Figure S16, Supporting Information).

## 3. Conclusion

In conclusion, this work shows that BOS) fibers prepared by side-by-side electrospinning are a versatile platform for the regioselective modification of electrospun fibers on the micron scale. The functional, hydrophilic beads can be selectively modified with a fluorescence dye and catalytically active AuNP. AuNP decorated BOS fiber nonwovens have proven high performance in continuous flow catalysis, combining a low-pressure drop across the nonwoven with high TOF values (up to  $\approx 90 \text{ h}^{-1}$ ) and excellent reusability. The flexibility of side-by-side electrospinning opens numerous possibilities for different material combinations, which can be employed for constructing tailor-made BOS fibers. The simple modification of the activated ester-based bead polymer allows the targeted synthesis of polymers for various applications like filtration or tissue engineering. This might stimulate further research on the fabrication of BOS fibers and explore more modifications and innovative applications.

# **Supporting Information**

Supporting Information is available from the Wiley Online Library or from the author.

## **Acknowledgements**

Financial support by Deutsche Forschungsgemeinschaft, grant number 632553. The authors acknowledge the Keylabs "Electron and Optical Microscopy" and "Synthesis and Molecular Characterization" of the Bavarian Polymer Institute (University of Bayreuth) for providing access to the electron microscopy and Raman imaging facilities and for their support during measurements. M.S. thanks the Elite Study Program Macromolecular Science within the Elite Network of Bavaria (ENB) and the University of Bayreuth Graduate School for support.

Open access funding enabled and organized by Projekt DEAL.

#### **Conflict of Interest**

The authors declare no conflict of interest.

## **Data Availability Statement**

The data that support the findings of this study are available in the supplementary material of this article.

## **Keywords**

electrospinning, heterogeneous catalysis, nanoparticles, regio-selective surface modification

Received: August 14, 2024 Published online: October 23, 2024

[1] a) A. Greiner, J. H. Wendorff, Angew. Chem., Int. Ed. 2007, 46, 5670;
b) M. Bognitzki, W. Czado, T. Frese, A. Schaper, M. Hellwig, M. Steinhart, A. Greiner, J. H. Wendorff, Adv. Mater. 2001, 13, 70; c) G. Duan, S. Jiang, V. Jérôme, J. H. Wendorff, A. Fathi, J. Uhm, V. Altstädt, M. Herling, J. Breu, R. Freitag, S. Agarwal, A. Greiner, Adv. Funct. Mater. 2015, 25, 2850.



www.advancedsciencenews.com



www.advmatinterfaces.de

- [2] a) J. Xue, T. Wu, J. Li, C. Zhu, Y. Xia, Angew. Chem., Int. Ed. 2019, 58, 3948; b) T. Wu, H. Li, J. Xue, X. Mo, Y. Xia, Angew. Chem., Int. Ed. 2019, 58, 16416.
- [3] a) A.-K. Müller, Z.-K. Xu, A. Greiner, Macromol. Mater. Eng. 2022, 307, 15; b) S. Zhang, H. Liu, N. Tang, N. Ali, J. Yu, B. Ding, ACS Nano 2019, 13, 13501; c) M. Burgard, D. Weiss, K. Kreger, H. Schmalz, S. Agarwal, H.-W. Schmidt, A. Greiner, Adv. Funct. Mater. 2019, 29, 1903166.
- [4] a) C. Zhu, X. Mu, P. A. van Aken, Y. Yu, J. Maier, Angew. Chem., Int. Ed. 2014, 53, 2152; b) S. Pazhaniswamy, S. A. Joshi, H. Hou, A. K. Parameswaran, S. Agarwal, Adv. Energy Mater. 2023, 13, 2202981.
- [5] a) G. Duan, M. Koehn-Serrano, A. Greiner, Macromol. Rapid Commun. 2017, 38, 1600511; b) M. Drummer, C. Liang, K. Kreger, S. Rosenfeldt, A. Greiner, H.-W. Schmidt, ACS Appl. Mater. Interfaces 2021, 13, 34818; c) J. Schöbel, M. Burgard, C. Hils, R. Dersch, M. Dulle, K. Volk, M. Karg, A. Greiner, H. Schmalz, Angew. Chem., Int. Ed. 2017, 56, 405.
- [6] a) M. Badmus, J. Liu, N. Wang, N. Radacsi, Y. Zhao, Nano Mater. Sci. 2021, 3, 213; b) Z. Lamberger, S. Zainuddin, T. Scheibel, G. Lang, ChemPlusChem 2023, 88, 202200371.
- [7] a) S. Jiang, Q. Jin, S. Agarwal, Macromol. Mater. Eng. 2014, 299, 1298;
   b) L. Peng, S. Jiang, M. Seuß, A. Fery, G. Lang, T. Scheibel, S. Agarwal, Macromol. Mater. Eng. 2016, 301, 48.

- [8] G. Lang, C. Grill, T. Scheibel, Angew. Chem., Int. Ed. 2022, 61, e202115232.
- [9] J. Zhang, X. Zha, G. Liu, H. Zhao, X. Liu, L. Zha, *Mater. Horiz.* 2024, 11, 1944.
- [10] J. Knapczyk-Korczak, J. Zhu, D. P. Ura, P. K. Szewczyk, A. Gruszczyński, L. Benker, S. Agarwal, U. Stachewicz, ACS Sustain. Chem. Eng. 2021, 9, 180.
- [11] M. Gernhardt, L. Peng, M. Burgard, S. Jiang, B. Förster, H. Schmalz, S. Agarwal, Macromol. Mater. Eng. 2018, 303, 243.
- [12] J. D. McGraw, J. Li, D. L. Tran, A.-C. Shi, K. Dalnoki-Veress, Soft Matter 2010, 6,1258.
- [13] Y. Liu, S. Tas, K. Zhang, W. M. de Vos, J. Ma, G. J. Vancso, *Macro-molecules* 2018, 51, 8435.
- [14] Z. Wang, C. Zhao, Z. Pan, J. Colloid Interface Sci. 2015, 441, 121.
- [15] Z. Song, K. Wang, C. Gao, S. Wang, W. Zhang, Macromolecules 2016, 49, 162.
- [16] S. Kaur, S. Sundarrajan, D. Rana, T. Matsuura, S. Ramakrishna, J. Membr. Sci. 2012, 392, 101.
- [17] P. Hervés, M. Pérez-Lorenzo, L. M. Liz-Marzán, J. Dzubiella, Y. Lu, M. Ballauff, Chem. Soc. Rev. 2012, 41, 5577.
- [18] G. Lin, J. Cai, Y. Sun, Y. Cui, Q. Liu, I. Manners, H. Qiu, Angew. Chem., Int. Ed. 2021, 60, 24637.